

Density distributions of tune shifts from space charge or beam-beam interactions in Gaussian bunches

Tanaji Sen *

Fermi National Accelerator Laboratory, Batavia, IL 60510

Abstract

The amplitude dependent tune shifts from either space charge or beam-beam interactions are calculated analytically with the inclusion of synchrotron oscillations and multiple interactions around the ring. Simpler formulae are derived under limits of bunches longer than the transverse sizes, equal and unequal transverse sizes etc. This is used to derive semi-analytical forms for the density distribution of the tune shifts. The tune spread and the density distribution are needed to understand beam decoherence or Landau damping with either interaction. The tune footprints due to space charge in IOTA are simulated using pyorbit and found to be in good agreement with the theoretical predictions.

1 Introduction

The space charge interaction in a low energy synchrotron and the beam-beam interaction in a collider are the dominant contributors to the incoherent tune spread in these machines. In this report we calculate first the incoherent amplitude dependent transverse tune shifts in 2D in Gaussian beams due to either interaction. We generalize these tune shifts to include the effects of synchrotron oscillations and especially in the case of space charge, we also include the contributions of the interactions from multiple locations around the ring. Next we calculate the beam density distributions as a function of these tuneshifts. These density distribution is needed to determine beam stability in different conditions. In terms of scaled tuneshifts (defined in Section 3), the density distribution has exactly the same form for both space charge and beam-beam interactions. However, the role of

*tsen@fnal.gov

the tune spread and the density in determining beam stability is different in the two interactions. The beam-beam interactions act as an external source of tune spread and can consequently be used to provide Landau damping [2] while with space charge interactions, an external driving source such as octupoles [1] or perhaps electron lenses [3] are required for Landau damping. Nevertheless even with space charge, the contribution from the internal tune spread and the density distribution have to be included in determining beam stability. Another use of the incoherent tune spread with either interaction is finding the beam decoherence time when the centroid is offset from the center e.g. due to a dipole kick.

. The calculation of tune shifts due to head-on beam-beam interactions in one dimension was reported in [4] while the fully 2D calculation of the tune spreads, resonance driving terms etc were done e.g in [5]. These were then generalized to long-range interactions [6], these were of greater interest in the Tevatron. The expressions for head-on interactions are easily found by taking appropriate limits. We note that the space charge tune shifts with amplitude for round beams without synchrotron oscillations were calculated in [7] which used some of the methods in [5]. The density distribution was extracted from numerical simulations, but insufficient sampling of the beam core led to an incorrect form for the density, especially close to the core where the space charge tune shift is largest. Our method is semi-analytical, in that numerical inversion of analytical functions followed by interpolation to obtain smooth functions is required. We also check that the zeroth to second moments of the distribution are preserved.

2 Incoherent tune shifts with synchrotron oscillations

Here we consider the tune shifts with amplitude due to a Hamiltonian with linear transverse motion, longitudinal motion in an rf bucket and either a space charge interaction or a beam-beam interaction. In this section, we consider first the Hamiltonian with a space charge interaction experienced by a Gaussian distribution in three space dimensions. At the end of this section, we consider the beam-beam interaction and show that the tuneshift with amplitude scaled by the zero amplitude tune shift has the same form as with space charge. The Hamiltonian in the lab frame can be written in dimensionless form as

$$H = \frac{1}{2}((x')^2 + (y')^2 + K_x x^2 + K_y y^2) + \frac{e}{\beta^2 \gamma m_0 c^2} (V_{rf} + V_{sc}) \quad (2.1)$$

where V_{rf} is the rf cavity voltage wave form and V_{SC} is the electric potential due to the space charge measured in the lab frame. Transforming to action-angle variables in the transverse planes, as e.g.

$$x = \sqrt{2\beta_x J_x} \cos \phi_x, \quad x' = \sqrt{2J_x} \left[\sqrt{\frac{1}{\beta_x}} \sin \phi_x - 2\alpha_x \cos \phi_x \right] \quad (2.2)$$

this reduces the linear part of the transverse Hamiltonian to

$$H_{\perp,0} = \frac{1}{R} (v_{x,0} J_x + v_{y,0} J_y) \quad (2.3)$$

where $(\nu_{x,0}, \nu_{y,0})$ are the tunes of the linear lattice and R is the machine radius.

Consider a Gaussian distribution in 3 space dimensions for a bunch; the same bunch experiencing its space charge field or the opposing bunch for the case of beam-beam interactions

$$\psi(x, y, z) = \frac{Ne}{(2\pi)^{3/2} \sigma_x \sigma_y \sigma_z} \exp\left[-\frac{x^2}{2\sigma_x^2} - \frac{y^2}{2\sigma_y^2} - \frac{z^2}{2\sigma_z^2}\right] \quad (2.4)$$

where $\sigma_x, \sigma_y, \sigma_z$ are the rms bunch dimensions. The solution of Poisson's equation $\nabla^2 V = -\psi/\epsilon_0$ leads to the following solution for the electric scalar potential [8]

$$V(x, y, z) = \frac{1}{4\pi\epsilon_0} \frac{Ne}{\pi^{1/2}\gamma} \int_0^\infty dq \frac{1}{\sqrt{(2\sigma_x^2 + q)(2\sigma_y^2 + q)(2\gamma^2\sigma_z^2 + q)}} \left[1 - \exp\left(-\frac{x^2}{2\sigma_x^2 + q} - \frac{y^2}{2\sigma_y^2 + q} - \frac{\gamma^2 z^2}{2\gamma^2\sigma_z^2 + q}\right) \right] \quad (2.5)$$

where the coordinates (x, y, z) and the rms sizes $(\sigma_x, \sigma_y, \sigma_z)$ are measured in the rest frame. The complete Hamiltonian in three degrees of freedom (3D) after scaling by R is

$$H = \nu_{x,0} J_x + \nu_{y,0} J_y + \frac{eR}{\beta^2 \gamma m_0 c^2} V_{rf}(\delta p/p, z) + C_{SC} \bar{V}(x, y, z) \quad (2.6)$$

$$C_{SC} = \frac{N_p r_p}{\pi^{1/2} \beta^2 \gamma^2} \quad (2.7)$$

$$\bar{V}_{sc}(x, y, z) = \int_0^\infty dq \frac{1}{\sqrt{(2\sigma_x^2 + q)(2\sigma_y^2 + q)(2\gamma^2\sigma_z^2 + q)}} \left[1 - \exp\left(-\frac{x^2}{2\sigma_x^2 + q} - \frac{y^2}{2\sigma_y^2 + q} - \frac{\gamma^2 z^2}{2\gamma^2\sigma_z^2 + q}\right) \right] \quad (2.8)$$

where $r_p = e^2/(4\pi\epsilon_0 m_0 c^2)$ is the classical particle radius. length. The tunes follow from the derivatives of the angle-averaged Hamiltonian

$$\nu_x = \frac{\partial}{\partial J_x} \langle H \rangle, \quad \langle H \rangle = \frac{1}{(2\pi)^2} \int d\phi_x d\phi_y H \quad (2.9)$$

We will write only the expressions in x , the one for y can be found by the replacement $x \leftrightarrow y$. Our focus is on the transverse tune shifts with amplitude, thus we ignore dominantly longitudinal effects such as longitudinal space charge effects. We also do not consider the momentum dependence of the transverse tunes or the modulation of the revolution period by the synchrotron oscillations, these do not have a noticeable effect on the dynamics in IOTA because of the small synchrotron tune. We do include the impact of synchrotron oscillations on the transverse dynamics via the nonlinear interaction potential. With these assumptions, the transverse tune shifts are given by

$$\Delta \nu_x = RC_{SC} \frac{\partial}{\partial J_x} \langle \bar{V} \rangle_{\phi_x, \phi_y, \phi_z, s} \quad (2.10)$$

where the averaging is done over all three angles and over s , the length along the ring. Hence after using action-angle variables,

$$\Delta v_x = RC_{SC} \int_0^\infty dq \frac{1}{\sqrt{(2\sigma_x^2 + q)^3 (2\sigma_y^2 + q) (2\gamma^2 \sigma_z^2 + q)}} 2\beta_x \cos^2 \phi_x \exp \left[-\frac{2\beta_x J_x \cos^2 \phi_x}{2\sigma_x^2 + q} - \frac{y^2}{2\sigma_y^2 + q} - \frac{\gamma^2 z^2}{2\gamma^2 \sigma_z^2 + q} \right]$$

Change the integration variable from q to a dimensionless variable u as

$$u = \frac{2\sigma_x^2}{(2\sigma_x^2 + q)}, \Rightarrow q = \frac{2\sigma_x^2}{u} - 2\sigma_x^2$$

This converts the infinite range of integration over q to a finite range of integration over u . Hence

$$\Delta v_x = \frac{RC_{SC} \beta_x}{2^{1/2} \sigma_x^2 \gamma \sigma_z} \int_0^1 du \left\langle \cos^2 \phi_x \left[\frac{1}{[(\sigma_y^2/\sigma_x^2 - 1)u + 1]} \frac{u}{[(1 - \sigma_x^2/\gamma^2 \sigma_z^2)u + \sigma_x^2/\gamma^2 \sigma_z^2]} \right]^{1/2} \exp \left[-\frac{2\beta_x J_x \cos^2 \phi_x}{2\sigma_x^2} u - \frac{2\beta_y J_y \cos^2 \phi_y}{2\sigma_y^2} \frac{u}{2\sigma_y^2 [(1 - \sigma_x^2/\sigma_y^2)u + \sigma_x^2/\sigma_y^2]} - \frac{\gamma^2 z^2 u}{2\gamma^2 \sigma_z^2 [(1 - \sigma_x^2/\gamma^2 \sigma_z^2)u + \sigma_x^2/\gamma^2 \sigma_z^2]} \right] \right\rangle_{\phi_x, \phi_y, s} \quad (2.11)$$

In order to make progress, we need to assume that the longitudinal motion is simple harmonic. This implies that the rf cavity force be linear or equivalently that the cosine term in V_{rf} be approximated by its Taylor expansion keeping only up to the quadratic term. Writing the coordinates (x, y, z) in terms of dimensionless amplitudes (a_x, a_y, a_z) and the corresponding rms sizes $(\sigma_x, \sigma_y, \sigma_z)$

$$x = a_x \sigma_x \cos \phi_x, \quad y = a_y \sigma_y \cos \phi_y, \quad z = a_z \sigma_z \cos \phi_z \quad (2.12)$$

We use the integral representation of I_0

$$I_0(w) = \frac{1}{\pi} \int_0^\pi d\theta \exp[\pm w \cos \theta] = \frac{1}{2\pi} \int_0^{2\pi} d\theta \exp[\pm w \cos 2\theta] \quad (2.13)$$

The integrals in the phase averages over ϕ_x, ϕ_y, ϕ_z are of the form

$$\frac{1}{2\pi} \int_0^{2\pi} d\phi \exp[-w \cos^2 \phi] = \exp[-\frac{1}{2}w] I_0(\frac{1}{2}w)$$

$$\frac{1}{2\pi} \int_0^{2\pi} d\phi \cos^2 \phi \exp[-w \cos^2 \phi] = \frac{1}{2} \exp[-\frac{1}{2}w] [I_0(\frac{1}{2}w) - I_1(\frac{1}{2}w)]$$

Gathering all terms together, the final expression is

$$\begin{aligned}
\Delta v_x(a_x, a_y, a_z) &= C_{SC} \frac{R}{2\sqrt{2}\gamma\sigma_z\epsilon_x} \int_0^1 du \exp\left[-\frac{a_x^2 u}{4}\right] \left[I_0\left(\frac{a_x^2 u}{4}\right) - I_1\left(\frac{a_x^2 u}{4}\right) \right] \exp\left[-\frac{a_y^2 u}{4}\right] \exp\left[-\frac{a_z^2 u}{4}\right] \\
&\quad \times \left\langle \left[\frac{1}{[(\sigma_y^2/\sigma_x^2 - 1)u + 1]} \frac{u}{[(1 - \sigma_x^2/\gamma^2\sigma_z^2)u + \sigma_x^2/\gamma^2\sigma_z^2]} \right]^{1/2} \right. \\
&\quad \left. \times I_0\left(\frac{a_y^2}{4} \frac{u}{(1 - \sigma_x^2/\sigma_y^2)u + \sigma_x^2/\sigma_y^2}\right) I_0\left(\frac{a_z^2 u}{4[(1 - \sigma_x^2/\gamma^2\sigma_z^2)u + \sigma_x^2/\gamma^2\sigma_z^2]}\right) \right\rangle_s
\end{aligned} \tag{2.14}$$

From this general expression, we can obtain the tuneshifts for special cases.

2.1 Bunch length longer than the transverse sizes

Using the general expression Eq.(2.14) in this limit where the transverse sizes are both negligibly small compared to the bunch length, i.e. $(\sigma_x, \sigma_y) \ll \sigma_z$ we find

$$\begin{aligned}
\Delta v_x(a_x, a_y, a_z) &= \Delta v_{x,SC} \left\langle \int_0^1 du \exp\left[-\frac{a_z^2 u}{4}\right] I_0\left(\frac{a_z^2 u}{4}\right) \exp\left[-\frac{a_x^2 u}{4}\right] \left[I_0\left(\frac{a_x^2 u}{4}\right) - I_1\left(\frac{a_x^2 u}{4}\right) \right] \exp\left[-\frac{a_y^2 u}{4}\right] \right. \\
&\quad \left. \times \left[\frac{1}{[(\sigma_y^2/\sigma_x^2 - 1)u + 1]} \right]^{1/2} I_0\left(\frac{a_y^2}{4} \frac{u}{(1 - \sigma_x^2/\sigma_y^2)u + \sigma_x^2/\sigma_y^2}\right) \right\rangle_s
\end{aligned} \tag{2.15}$$

Eq.(2.15) and a similar one for Δv_y (with $x \leftrightarrow y$) are of the form which is generally applicable for bunches in hadron synchrotrons, even the low energy machines where $\gamma \simeq 1$.

The tuneshift at the origin is

$$\begin{aligned}
\Delta v_{x,SC}(0, 0, 0) &= \frac{RC_{SC}}{2\sqrt{2}\gamma\epsilon_x\sigma_z} \int_0^1 du \left\langle \left[\frac{1}{[(\sigma_y^2/\sigma_x^2 - 1)u + 1]} \right]^{1/2} \right\rangle_s \\
&= \frac{RC_{SC}}{\sqrt{2}\gamma\epsilon_x\sigma_z} \left\langle \frac{1}{1 + \sigma_y/\sigma_x} \right\rangle_s
\end{aligned} \tag{2.16}$$

Substituting the expression for C_{SC} and assuming round beams at all locations, we obtain

$$\Delta v_{x,SC} = \frac{N_p r_p}{\beta^2 \gamma^2} \frac{R}{2\sqrt{2}\pi\gamma\sigma_z\epsilon_x} = \frac{r_p}{\beta \gamma^2 \epsilon_{x,N}} \lambda_G R, \quad \lambda_G = \frac{N_p}{2\sqrt{2}\pi\sigma_z} \tag{2.17}$$

where we used $\epsilon_{x,N} = \beta\gamma\epsilon_x$ and λ_G is the longitudinal density. These are the standard expressions for the space charge tune shift parameters for Gaussian bunches. With a coasting bunch, the longitudinal density is $\lambda = N_p/(2\pi R)$.

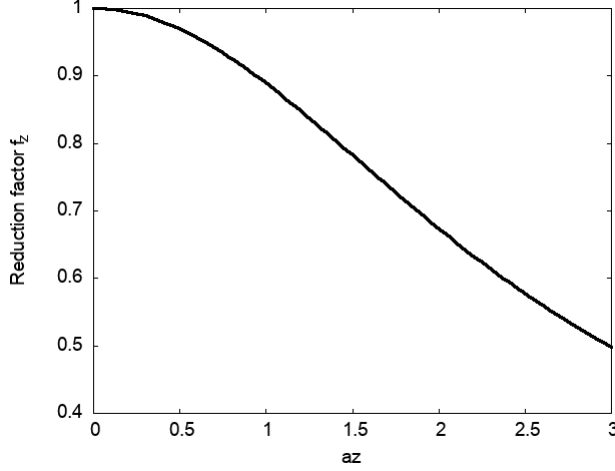


Figure 1: Correction factor f_z for the reduction of the zero amplitude tune shift as a function of the dimensionless amplitude a_z .

The zero amplitude tune shifts for non-round beams can be written as

$$\Delta v_x(0,0,0) = 2 \left\langle \frac{1}{\sigma_y/\sigma_x + 1} \right\rangle_s \Delta v_{x,SC}, \quad \Delta v_y(0,0,0) = 2 \left\langle \frac{1}{\sigma_x/\sigma_y + 1} \right\rangle_s \Delta v_{y,SC} \quad (2.18)$$

These equations include the variation of beam sizes around the ring.

At zero transverse amplitude in this limit of both long and round bunches

$$\Delta v_x(0,0,a_z)|_{Long,round} = \Delta v_{x,SC} \int_0^1 du \exp\left[-\frac{a_z^2 u}{4}\right] I_0\left(\frac{a_z^2 u}{4}\right) \equiv f_z \Delta v_{x,SC} \quad (2.19)$$

$$f_z = \exp\left[-\frac{a_z^2}{4}\right] \left(I_0\left(\frac{a_z^2}{4}\right) + I_1\left(\frac{a_z^2}{4}\right) \right) \quad (2.20)$$

where f_z is the correction factor which describes the impact of synchrotron oscillations. Hence f_z plotted in Fig. 1 shows that the small amplitude tune shifts due to space charge of a longitudinal slice decreases with distance z , falling by half at $a_z = 3$ corresponding to the edge of the bucket. The caveat is that the longitudinal motion is not simple harmonic; nevertheless this curve should be accurate at smaller amplitudes. The small amplitude particles can oscillate over different synchrotron amplitudes; we can average over the full range of these amplitudes. Assuming a Gaussian distribution in a_z , we find

$$\langle f_z \rangle = \frac{\sqrt{2}(\pi^2 - 2\Gamma[3/4]^4)}{\pi^{3/2}\Gamma[3/4]^2} \simeq 0.91 \quad (2.21)$$

We find that synchrotron oscillation reduces the small amplitude tune shift by about 10%. However since synchrotron oscillations have a much longer time scale than betatron oscillations, this average value $\langle f_z \rangle$ may not be a useful indicator of their impact.

Zero synchrotron amplitude $a_z = 0$ with arbitrary transverse sizes

$$\begin{aligned} \Delta v_x(a_x, a_y, 0)|_{Long} = \Delta v_{x,SC} \left\langle \int_0^1 du \exp\left[-\frac{a_x^2 u}{4}\right] \left[I_0\left(\frac{a_x^2 u}{4}\right) - I_1\left(\frac{a_x^2 u}{4}\right) \right] \right. \\ \left. \times \exp\left[-\frac{a_y^2 u}{4}\right] \left[\frac{1}{[(\sigma_y^2/\sigma_x^2 - 1)u + 1]} I_0\left(\frac{a_y^2 u}{4} \frac{u}{(1 - \sigma_x^2/\sigma_y^2)u + \sigma_x^2/\sigma_y^2}\right) \right] \right\rangle_s \end{aligned} \quad (2.22)$$

We observe that when the beams are not round, the tunes shift depends on the variation of the relative beam size σ_y/σ_x around the ring. The average over the ring can be calculated exactly with an integral evaluation at several points along the ring or approximately by replacing the average over the function by the function of the averaged argument. This approach would require a single integral and would be computationally faster. The quality of this approximation will be evaluated in Section 4 for IOTA parameters.

With the further assumption of round bunches everywhere, the above simplifies to

$$\begin{aligned} \Delta v_x(a_x, a_y, a_z)|_{Long,round} = \Delta v_{x,SC} \int_0^1 du \exp\left[-\frac{a_z^2 u}{4}\right] I_0\left(\frac{a_z^2 u}{4}\right) \\ \times \exp\left[-\frac{a_x^2 u}{4}\right] \left[I_0\left(\frac{a_x^2 u}{4}\right) - I_1\left(\frac{a_x^2 u}{4}\right) \right] \exp\left[-\frac{a_y^2 u}{4}\right] I_0\left(\frac{a_y^2 u}{4}\right) \end{aligned} \quad (2.23)$$

In most machines the bunch is not round everywhere in the ring, nevertheless Eq.(2.23) can be used as a first approximation for the tunes shift with amplitude.

In Section 4 we evaluate the tune shifts for IOTA parameters and consider the impact of synchrotron oscillations and the round beams approximation on the transverse tune shifts.

2.2 Beam-beam tune shifts

The beam-beam tune footprint can be found in a similar fashion as above. The major difference is that in a collider, the particles all move at very relativistic speeds, so $\beta \simeq 1, \gamma \gg 1$. Consequently there is a large increase in the transverse fields in going from the rest frame to the lab frame due to the Lorentz boost while the longitudinal fields are unchanged.

$$\mathbf{E}_{\perp,lab} \simeq \gamma \mathbf{E}_{\perp,rest} = -\gamma \nabla_{\perp} V_{BB}, \quad E_{z,lab} = E_{z,rest}, \quad B_{x,lab} = \frac{E_{y,lab}}{\beta}, \quad B_{y,lab} = -\frac{E_{x,lab}}{\beta} \quad (2.24)$$

Here V_{BB} is the scalar potential for the beam-beam interaction and is the same as V_{SC} except that the beam parameters are of the opposing bunch. The net force due to the electric and magnetic fields are in the same direction for beam-beam interactions and oppose each other with space-charge. While the space charge forces act radially outward in all directions, the beam-beam forces are almost entirely in the transverse plane emanating from a squashed

pancake like disc traveling with the opposing beam. In most circumstances we can think of the opposing beam as being point-like along the direction of motion and the beam-beam potential as effectively two dimensional. The longitudinal density has a role to play in beam-beam interactions in effects such as phase averaging in long bunches [9, 10] or when hourglass effects [11] or crossing angles are introduced; see [12] for a recent calculation of the luminosity and beam-beam tune shifts with both these effects in a Higgs factory $e^+ - e^-$ collider.

In most cases where the beam-beam interaction is 2D, the results of Section 2.1 are applicable here because $\gamma \gg 1$. Following the same procedure as in obtaining Eq. (2.18) leads to the beam-beam tune shift at the origin

$$\Delta v_{x,BB} = \frac{r_p N_p \beta_x^*}{2\pi\gamma} \frac{1}{\sigma_x^*(\sigma_x^* + \sigma_y^*)}, \quad \Delta v_{y,BB} = \frac{r_p N_p \beta_y^*}{2\pi\gamma} \frac{1}{\sigma_y^*(\sigma_x^* + \sigma_y^*)} \quad (2.25)$$

where $\beta_x^*, \beta_y^*, \sigma_x^*, \sigma_y^*$ are the values at the IP and we assumed that the beam parameters are the same at all the IPs.

The important point here is that both the space charge and the beam-beam potential have the same dependence on the transverse amplitudes, consequently the two footprints are the same if we scale out the zero amplitude tune shifts. Thus, the horizontal beam-beam tune shift at transverse amplitudes (a_x, a_y) can be written down using Eq.(2.22)

$$\begin{aligned} \Delta v_{x,BB}(a_x, a_y) = & \Delta v_{x,BB} \int_0^1 du \exp\left[-\frac{a_x^2 u}{4}\right] \left[I_0\left(\frac{a_x^2 u}{4}\right) - I_1\left(\frac{a_x^2 u}{4}\right) \right] \exp\left[-\frac{a_y^2 u}{4}\right] \\ & \times \left[\frac{1}{[(\sigma_y^2/\sigma_x^2 - 1)u + 1]} I_0\left(\frac{a_y^2}{4} \frac{u}{(1 - \sigma_x^2/\sigma_y^2)u + \sigma_x^2/\sigma_y^2}\right) \right] \end{aligned} \quad (2.26)$$

A similar expression holds in the vertical plane.

3 Density distribution in tunes

We saw in the previous section that the beam and machine parameters describing the space charge and beam-beam tune shifts are all included in the zero amplitude tune shifts $\Delta v_{x,SC}, \Delta v_{y,SC}$. It is therefore useful to describe the universal functions of the dimensionless amplitudes as

$$\xi_x(a_x, a_y, a_z) = \frac{\Delta v_x(a_x, a_y, a_z)}{\Delta v_{x,SC}}, \quad \xi_y(a_x, a_y, a_z) = \frac{\Delta v_y(a_x, a_y, a_z)}{\Delta v_{y,SC}} \quad (3.1)$$

The functions ξ_x, ξ_y are universal in the sense that their behavior describes the amplitude dependence for any machine. In this section we consider the distribution assuming a Gaussian distribution in phase space.

3.1 Density distribution in 1D

We start with the tune density distribution in 1D. for the sake of clarity. The density in action J_x is transformed to the dimensionless amplitude variable α_x as

$$\rho(J_x) = \frac{1}{\epsilon_x} \exp[-\frac{J_x}{\epsilon_x}] = \frac{1}{\epsilon_x} \exp[-2\alpha_x], \quad \alpha_x = \frac{a_x^2}{4} = \frac{J_x}{2\epsilon_x} \quad (3.2)$$

$$\rho(\alpha_x) = \rho(a_x) \left[\frac{\partial \alpha_x}{\partial a_x} \right]^{-1} = a_x \exp[-\frac{1}{2} a_x^2] [a_x/2]^{-1} = 2 \exp[-2\alpha_x] \quad (3.3)$$

Now we need to transform from the amplitude to the scaled tuneshift which implies

$$\rho(\xi_x) = \frac{\rho(\alpha_x)}{d\xi_x/d\alpha_x} = \frac{1}{2} \exp[-2\alpha_x] \left[\int_0^1 du u [H'_0(\alpha_x u) - H'_1(\alpha_x u)]^{-1} \right] \quad (3.4)$$

$$H_n(z) \equiv \exp[-z] I_n(z) \quad (3.5)$$

Hence, using the tuneshift expression in 1D

$$\xi_x(\alpha_x) = \int_0^1 du [H_0(\alpha_x u) - H_1(\alpha_x u)] \quad (3.6)$$

$$\rho(\xi_x) = \rho(\alpha_x) \left[\frac{\partial \xi_x}{\partial \alpha_x} \right]^{-1} = 2 \exp[-2\alpha_x] \left[\int_0^1 du u [H'_0(\alpha_x u) - H'_1(\alpha_x u)]^{-1} \right] \quad (3.7)$$

$$\equiv 2 \frac{\exp[-2\alpha_x]}{\text{Jac}(\alpha_x, \xi_x)} \quad (3.8)$$

Here $\text{Jac}(\alpha_x, \xi_x)$ is the Jacobian of the transformation from $\alpha_x \rightarrow \xi_x$. Eq.(3.6) defines ξ_x as a function of α_x . Inverting this relation (numerically) defines α_x as a function of ξ_x . We denote this function $\alpha_F(\xi_x)$. Inserting this function back into Eq.(3.8) yields the functional form

$$\rho(\xi_x) = 2 \frac{\exp[-2\alpha_F(\xi_x)]}{\text{Jac}(\alpha_F(\xi_x))} \quad (3.9)$$

In 1D, the inverse function is straightforward to obtain. Fig. 2 shows plots of the function $\xi_x(\alpha_x)$ and the inverse function $\alpha_F(\xi_x)$ which resembles a one-sided delta function.

The p th moment of the tuneshift i.e. $\langle \xi_x^0 \rangle$ (the norm), $\langle \xi_x^1 \rangle$, $\langle \xi_x^2 \rangle$, ... should agree in any coordinate system used for the density distribution. We can use this to test the accuracy of the distribution in ξ_x . The two lowest moments can be calculated analytically using the known functional forms in terms of α_x .

$$\int_0^1 \rho(\xi_x) d\xi_x = \int_0^\infty \rho(\alpha_x) d\alpha_x = 2 \int_0^\infty \exp[-2\alpha_x] d\alpha_x = 1 \quad (3.10)$$

$$\begin{aligned} \langle \xi_x \rangle &= \int_0^\infty \xi(\alpha_x) \rho(\alpha_x) d\alpha_x = 2 \int_0^\infty \exp[-2\alpha_x] d\alpha_x \int_0^1 du [H_0(\alpha_x u) - H_1(\alpha_x u)] \\ &= 2 \int_0^\infty d\alpha_x \int_0^1 du \exp[-(2+u)\alpha_x] [I_0(\alpha_x u) - I_1(\alpha_x u)] \end{aligned} \quad (3.11)$$

Using the integration result from the table of integrals in [13]

$$\int_0^\infty e^{-\alpha z} I_p(\beta z) dz = \frac{\beta^p}{\sqrt{\alpha^2 - \beta^2}(\alpha + \sqrt{\alpha^2 - \beta^2})^p} \quad (3.12)$$

Doing the integral over α_x first followed by the integration over u , we find

$$\begin{aligned} \langle \xi_x \rangle &= \int_0^\infty d\alpha_x \exp[-(2+u)\alpha_x] [I_0(\alpha_x u) - I_1(\alpha_x u)] \\ &= \int_0^1 du \left[\frac{1}{\sqrt{1+u}} - \frac{1}{\sqrt{1+u}} \frac{u}{(1+\sqrt{1+u})^2} \right] \end{aligned} \quad (3.13)$$

$$= 4(\text{Arcsinh}[1] - \log[2]) = 0.752906 \quad (3.14)$$

Numerically the moments can also be calculated using either $\rho(\alpha_x)$ or using $\rho(\xi_x)$. The results are shown in Table 1 where Numerical 1 uses the first method and Numerical II uses the second method. The fact that the moments calculated numerically with Numerical II agrees exactly with the other methods gives confidence that the expression for the density distribution in tuneshift $\rho(\xi_x)$ is correct.

Finally, we calculate the median tuneshift which by definition is the value at which the number of particles is the same both above and below the median value ξ_M , i.e.

$$\int_0^{\xi_M} \rho(\xi_x) d\xi_x = \int_{\xi_M}^\infty \rho(\xi_x) d\xi_x = 0.5 \Rightarrow \xi_M = 0.783 \quad (3.15)$$

The density distribution $\rho(\xi_x)$ along with the average and median tuneshifts are indicated in the bottom plot of Fig. 2.

The 1D density vanishes in the range $a \leq \xi_x \leq 0.2$ and reaches a maximum at $\xi_x = 1$, as expected since that is also the region of maximum density.

3.2 Density distribution in 2D

The procedure is the same as in 1D, the details are slightly different because first a nonlinear equation in two variables has to be solved followed by a 2D interpolation is required. Let the density in tune space be $\rho(\xi_x, \xi_y)$. By the conservation of particle number,

$$\rho(\alpha_x, \alpha_y) d\alpha_x d\alpha_y = \rho(\xi_x, \xi_y) d\xi_x d\xi_y \quad (3.16)$$

which implies

$$\rho(\xi_x, \xi_y) = \rho(\alpha_x, \alpha_y) / \text{Jac}(\xi_x, \xi_y; \alpha_x, \alpha_y) \quad (3.17)$$

where

$$\text{Jac}(\xi_x, \xi_y; \alpha_x, \alpha_y) = \left\| \begin{array}{cc} \frac{\partial \xi_x}{\partial \alpha_x} & \frac{\partial \xi_x}{\partial \alpha_y} \\ \frac{\partial \xi_y}{\partial \alpha_x} & \frac{\partial \xi_y}{\partial \alpha_y} \end{array} \right\| \quad (3.18)$$

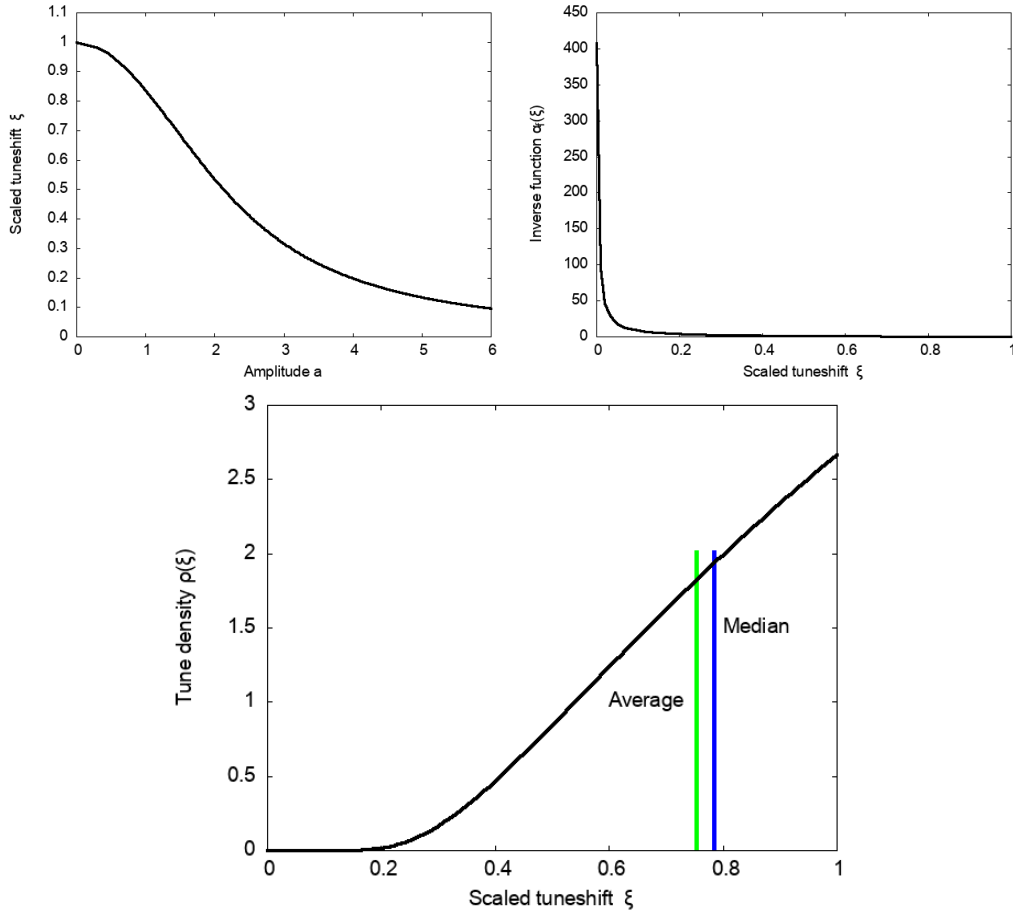


Figure 2: Top: Tune shift ξ as a function of the scaled amplitude $a_x = 2\sqrt{\alpha_x}$, a_x is the transverse amplitude in units of the rms size; Right: The inverse function $\alpha_x(\xi)$. Bottom: The density distribution as a function of the tuneshift.

	Analytical	Numerical I	Numerical II
	1D		
Normalization	1.0	1.0	1.0
$\langle \xi_x \rangle$	0.752906	0.752906	0.752906
$\langle \xi_x^2 \rangle$	N/A	0.597766	0.597766
$\xi_{x,rms}$	N/A	0.175782	0.175782
	2D		
Normalization	1.0	1.0	0.981
$\langle \xi_x \rangle$	0.633389	0.633389	0.629
$\langle \xi_x^2 \rangle$	N/A	0.4293	0.4596
$\xi_{x,rms}$	N/A	0.1678	0.253

Table 1: Moments of the density distribution calculated in different ways in 1D and 2D. The two numerical ways, labeled as I and II, describe using the density in amplitude space e.g. $\rho(\alpha_x, \alpha_y)$ and tune space respectively.

the density can be written as

$$\rho(\alpha_x, \alpha_y) = 4 \exp[-2\alpha_x - 2\alpha_y] \quad (3.19)$$

In terms of these variables, the scaled tune shifts are

$$\xi_x(\alpha_x, \alpha_y) = \int_0^1 du [H_0(\alpha_x u) - H_1(\alpha_x u)] H_0(\alpha_y u) \quad (3.20)$$

$$\xi_y(\alpha_x, \alpha_y) = \int_0^1 du H_0(\alpha_x u) [H_0(\alpha_y u) - H_1(\alpha_y u)] \quad (3.21)$$

The derivatives are found for example as

$$\frac{\partial \xi_x}{\partial \alpha_x} = \left(\int_0^1 du u H_0(\alpha_x u) [H_0'(\alpha_x u) - H_1'(\alpha_x u)] H_0(\alpha_y u) \right) \quad (3.22)$$

These can be used to write the density in tune space using Eqs. (3.17), (3.19), (3.18) in terms of ξ_x, ξ_y . Doing so yields

$$\rho(\xi_x, \xi_y) = 4 \frac{\exp[-2\alpha_x - 2\alpha_y]}{\text{Jac}(\xi_x, \xi_y; \alpha_x, \alpha_y)} \quad (3.23)$$

The RHS of this equation however is a function of the amplitudes (α_x, α_y) while what we want is a function of the scaled tune shifts (ξ_x, ξ_y) . That requires an inversion of Eqs. (3.20) and (3.21). It is done in two steps: (1) solving these nonlinear equations to find α_x, α_y as functions of ξ_x, ξ_y and (2) interpolating these to write these as smooth functions of ξ_x, ξ_y . Fig. 3 shows the complete density $\rho(\xi_x, \xi_y)$ as a function of ξ_x, ξ_y viewed from two different angles as well the projected density $\rho_x(\xi_x)$ on the ξ_x axis, which is obtained by integrating over the ξ_y axis, i.e.

$$\rho_x(\xi_x) = \int_0^1 d\xi_y \rho(\xi_x, \xi_y) \quad (3.24)$$

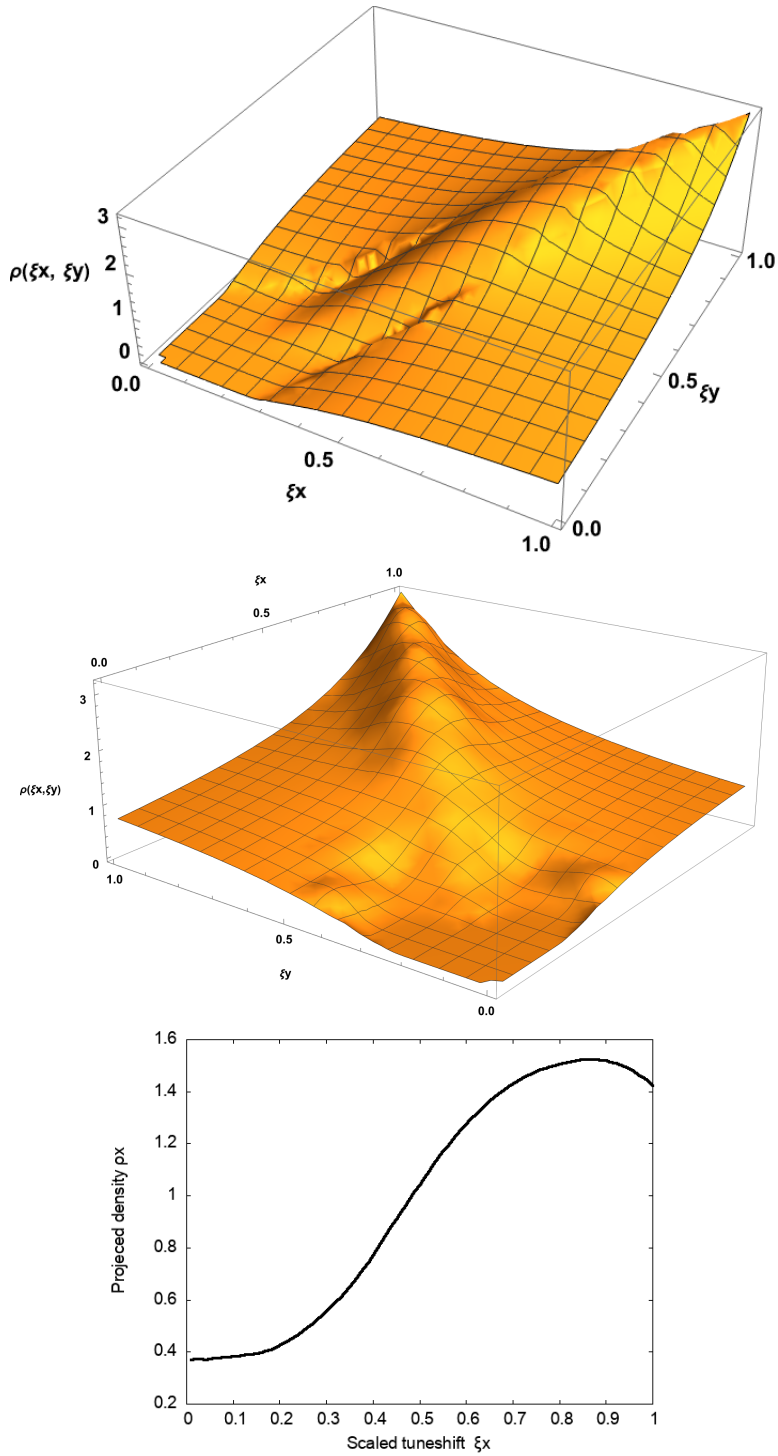


Figure 3: Top: Density $\rho(\xi_x, \xi_y)$ vs the scaled tune shifts ξ_x, ξ_y . : This plots shows the density from a different angle, it shows e.g. the density along the ξ_x and also along the ξ_x axes..Right: The projected density ρ_x along the ξ_x axis. It is non-zero at $\xi_x = 0$ and it has a maximum at a value less than $\xi_x = 1$.

The density is exactly symmetric along the $\xi_x = \xi_y$ axis, as it must be for round beams. The second plot shows that the density is zero at the origin and we observe that along either the ξ_x axis or the ξ_y axis the density is similar to the 1D density profile seen in Fig. 2. The projected density does not vanish at $\xi_x = 0$ and it has a maximum around $\xi_x = 0.9$ rather than at $\xi_x = 1$. A little thought shows that is true of any density that has a non-vanishing dependence on both α_x, α_y .

The moments of the distribution are found as before

$$\begin{aligned} \langle \xi_x \rangle &= \int_0^\infty d\alpha_x \int_0^\infty d\alpha_y \xi_x(\alpha_x, \alpha_y) \rho(\alpha_x, \alpha_y) \\ &= 4 \int_0^1 du \int_0^\infty d\alpha_x \int_0^\infty d\alpha_y [H_0(\alpha_x u) - H_1(\alpha_x u)] H_0(\alpha_y u) \exp[-2\alpha_x - 2\alpha_y] \end{aligned} \quad (3.25)$$

For the integration over α_y , we use the same integral result in Eq.(3.12) to obtain

$$\int_0^\infty H_0(\alpha_y u) \exp[-2\alpha_x - 2\alpha_y] d\alpha_y = \frac{1}{\sqrt{1+u}}$$

Combining this integration and doing the final integral over u , we find

$$\langle \xi_x \rangle = 4 \ln \left[\frac{2\sqrt{2}}{\sqrt{2}+1} \right] = 0.633389 \quad (3.26)$$

The moments are calculated numerically using both methods used for the 1D distribution, are shown in Table 1. The normalization is not quite unity with the second method. We attribute this $\sim 2\%$ error to numerical issues in the inversion and interpolation required to find the functions $\alpha_x(\xi_x, \xi_y), \alpha_y(\xi_x, \xi_y)$. This can be used to find the correct moments by dividing the raw moments by the normalization. With this correction, the error in the first moment is $\sim 0.7\%$ while the error in the second moment is 7% .

We briefly consider application of these results to beam stability with octupoles and space charge, a more detailed study will be reported elsewhere. Typically the stability is considered using the dispersion relation with a 2D betatron spread from both octupoles and space charge. This relation was used to derive stability curves [14] with a parabolic transverse density and a space charge tune spread linear in the actions to match the octupolar tune spread. It may be possible to use the exact space charge tune spread $\Delta v_{x,SC}(a_x, a_y) = \Delta v_{x,SC} \xi_z(a_x, a_y)$ to obtain stability curves for Gaussian bunches. The extension to 3D stability is in principle straightforward, using the 3D space charge tuneshifts $\xi_{x,y}(a_x, a_y, a_z)$. A more direct use of the density curves derived in this section would be to check the results derived from PIC simulations against the exact results obtained here.

IOTA proton parameters	
Circumference	39.97 [m]
Kinetic Energy	2.5 [MeV]
Maximum bunch intensity /current	$9 \times 10^{10} / 8$ [mA]
Transverse normalized rms emittance	(0.3, 0.3) [mm-mrad]
Betatron tunes	(5.3, 5.3)
Natural chromaticities	(-8.2, -8.1)
Average transverse beam sizes (rms)	(2.22, 2.22) [mm]
Kinematic γ / Transition γ_T	1.003 / 3.75
Rf voltage	400 [V]
Rf frequency / harmonic number	2.2 [MHz] / 4
Bucket wavelength	~ 10 [m]
Bucket half height in $\Delta p/p$	3.72×10^{-3}
rms bunch length	1.7 [m]
rms energy /momentum spread	$1.05 \times 10^{-5} / 1.99 \times 10^{-3}$

Table 2: Machine and beam parameters of the IOTA proton ring

4 Application to IOTA

IOTA is an accelerator that was designed to test the concept of nonlinear integrable lattices [15]. The R & D program with electrons and protons was discussed in [16]. The ring has been operated with electrons since commissioning began and several notable results have been achieved, including the demonstration of optical stochastic cooling [17]. Proton operation is scheduled to begin in 2024 when the concept of achieving high space charge tune shifts with a nonlinear integrable lattice will be tested.

In this section, we will evaluate the space charge footprints theoretically and compare with particle tracking. This is done in an otherwise completely linear lattice; we note that emittance growth and beam loss was studied in a partially integrable lattice with octupoles in [20]. Table 2 shows the relevant parameters of the IOTA proton ring. First, we consider whether the beam is sufficiently round everywhere in the ring for the round beam expressions for the footprint to be applicable. Fig. 4 shows the ratio of the vertical to horizontal beam sizes along the ring. The ratio varies between 0.5 to 5.0 with a mean value of 1.2. The mean value may not be relevant here, as the fluctuations are fairly large. We therefore use the general expression for the tune shifts but we also compare with the round beam forms as well as an approximation discussed in Section 2. We discuss first the theoretical footprints under the different assumptions discussed in Section II. In the limit of long bunches, which is valid for iOTA, we can use Eq.(2.14). This involves calculating the tune shift at each longitudinal location and averaging over the locations. This method requires doing an integration at each location. We can reverse the order and instead do the averaging first and

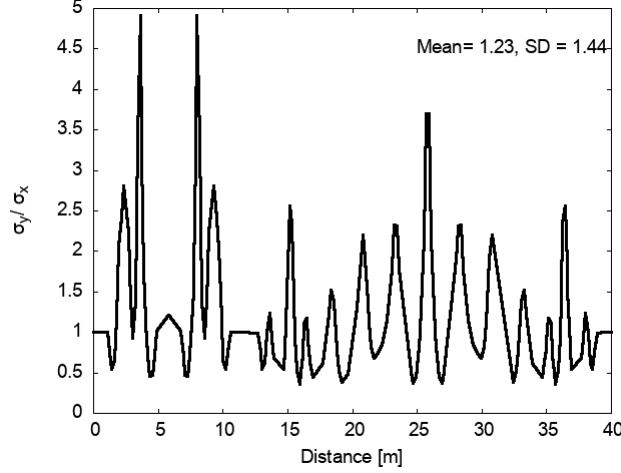


Figure 4: Ratio of σ_y/σ_x around the ring.

do a single integration instead.

$$\Delta v_x(a_x, a_y, a_z) = \Delta v_{x,SC} \int_0^1 du \left\{ \left\langle \exp\left[-\frac{a_z^2 u}{4}\right] I_0\left(\frac{a_z^2 u}{4}\right) \exp\left[-\frac{a_x^2 u}{4}\right] \left[I_0\left(\frac{a_x^2 u}{4}\right) - I_1\left(\frac{a_x^2 u}{4}\right) \right] \exp\left[-\frac{a_y^2 u}{4}\right] \right. \right. \\ \left. \left. \times \left[\frac{1}{[(\sigma_y^2/\sigma_x^2 - 1)u + 1]} \right]^{1/2} I_0\left(\frac{a_y^2}{4} \frac{u}{(1 - \sigma_x^2/\sigma_y^2)u + \sigma_x^2/\sigma_y^2}\right) \right\rangle_s \right\} \quad (4.1)$$

This reduces the time required for evaluation and we found that the differences in numerical values are negligible, at least in the case of IOTA.

The left plot in Fig. 5 shows a comparison of the footprints based on the general expression in Eq.(2.14), and that based on the round beam expression in Eq.(2.23). The differences are small; this is to be expected as IOTA has been designed to have axial symmetry almost everywhere in the ring in order to preserve integrability [15]. The right plot in this figure shows the footprints with synchrotron oscillations at two amplitudes $a_s = 1, 2$. As exported from Fig. 1, the total tunes shift at $a_s = 1$ is about 90% and at $a_s = 2$, the total tunes shift is 70% of the value at $a_s = 0$.

The theory of the tunes shifts assumes that the particles stay at constant amplitudes while executing betatron oscillations. This is not always true, especially at high intensities. We examine this assumption by testing emittance growth with pyorbit simulations [18]. Many details on the pyorbit simulations and their validation can be found in earlier reports [19, 20]. Detailed analysis had shown that there was good agreement between theory and simulations in all the tested regimes. In the simulations reported here, all machine nonlinearities were turned off, space charge was the only nonlinearity. The results reported in [19] showed that initial beam losses can be minimized by a process of slow initialization in which the charge per macroparticle is increased over about 40 turns to full value and the beam was injected into a lattice that was rms matched to equilibrium beam sizes. The PIC parameters that led to convergence were found to have the following values: number of

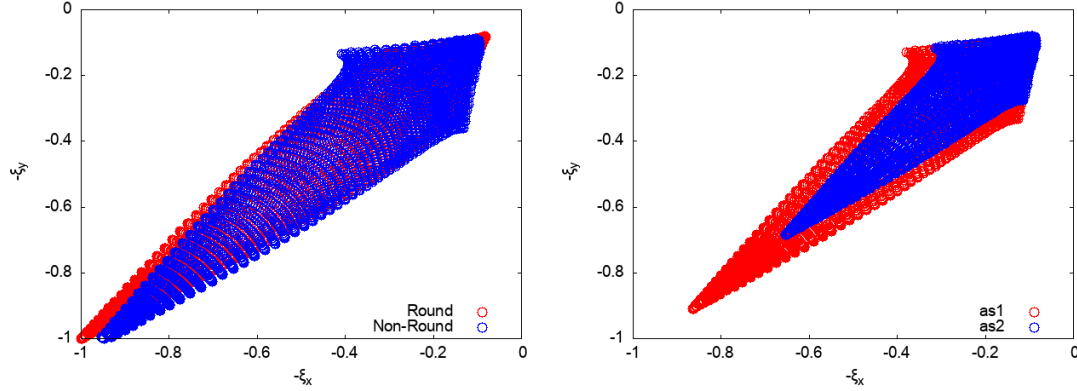


Figure 5: Left: Comparison of round and non-round footprints without synchrotron oscillations. Right: Footprints with synchrotron oscillation amplitudes of $1\sigma_s$ (in red) and $2\sigma_s$ (blue).

macroparticles = 5×10^5 , grid size = $128 \times 128 \times 5$, and the number of space charge kicks per betatron wavelength = 63. These values were used in the simulations discussed below.

It is not completely straightforward to compare space charge simulations with theory especially at high intensities. The simplest is to compare the small charge tune shifts. The complications arise from two effects Theory assumes that the tune shift is calculated at constant emittances, which is not the case as the space charge increases. The second complication is related to PIC simulations. It has been observed that this method causes orbits to be chaotic at small amplitudes close to the origin [21]. We dealt with the first issue by using the average emittance over the time used for the tuneshift calculation. For the second issue, we distribute particles over 100 different angles at the same small amplitude and average over the angles to reduce the fluctuations in the tune shift value. Another complication at high intensities is that because the FFT aliases tunes to be in the range 0 - 0.5, it cannot determine if the tunes are below or above the half integer when the space charge tune shift exceeds 0.5. We had determined the tune with the alternative method of counting the number of betatron oscillations over a thousand turns and found that the simulated tunes calculated both ways agreed well with each other and with theory [19].

At a low intensity of 10^9 particles/bunch, there are only fluctuations due to numerical noise in the PIC simulations. These are observed to be around 0.4%, which is close to the expected level $\sim 1/\sqrt{N} = 0.14\%$ with $N = 5 \times 10^5$. Fig. 6 shows the emittance change over a range of intensities; the last value 9×10^{10} corresponds to the maximum design bunch intensity. Since there is very little observable emittance growth at the lowest intensities in this range, we expect the simulated tunes to be close to theoretical values. However, the tune shifts are too small to be accurately computable with an FFT over ~ 1000 turns, especially to resolve the tune-shift for neighboring particles. At intermediate intensity of 10^{10} , there is a larger emittance growth pf $\sim 10\%$ while at 9×10^{10} , the emittance grows by nearly a factor of ten without slow initialization. The tune footprints are calculated using 5×10^5 macroparticles and using 5000 test particles distributed transversely from 0 - 5σ and with zero synchrotron amplitude. Fig. 7 shows the footprints at 10^{10} and 9×10^{10} intensities

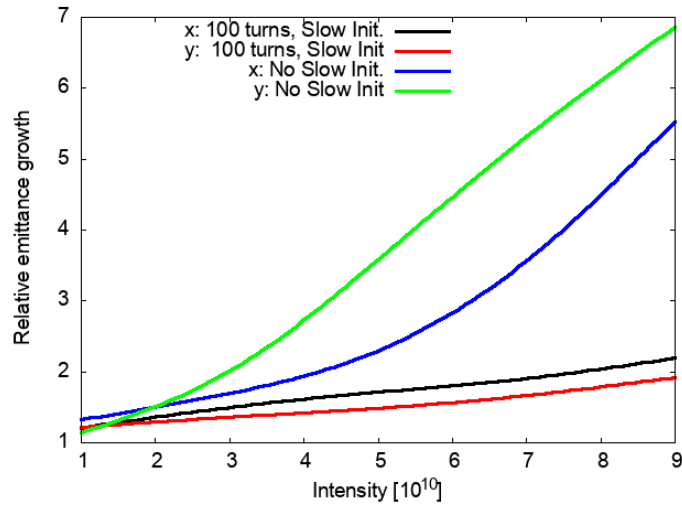


Figure 6: Relative emittance growth over 1000 turns as a function of the intensity for two conditions: without slow initialization and with a slow initialization of 100 turns.

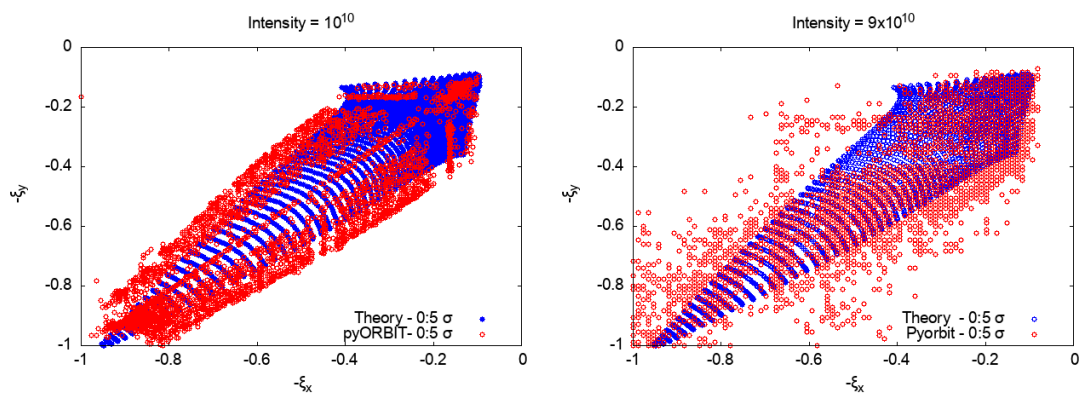


Figure 7: Footprints from Pyorbit tracking and theory with non-round beams. Left: Intensity = 10^{10} , Right: Intensity = 9×10^{10}

obtained with pyorbit simulations and compared with the theoretical values using Eq.(2.22). In both cases, we have scaled the numerical footprints by the maximum tuneshift, so the analytical and numerical footprints can be easily compared. At the lower intensity, the two footprints agree reasonably well although the simulated footprint is wider at amplitudes from 1 to 5σ . At the intensity of 9×10^{10} , the simulated footprint is even wider and the agreement is not as close, which is to be expected. The single most important reason for the increasing discrepancy is that the theory assumes that all particles move on invariant actions which is not true at high intensities. Nevertheless, the theoretical footprint can be useful both as a benchmark tool and also to quickly determine the important resonances that can be crossed by the footprint at a chosen working point.

5 Conclusions

We derived tune shifts with amplitude in terms of a universal dimensionless parameter under quite general conditions that are valid for space charge or beam-beam interactions. We included multiple interaction points and synchrotron oscillations. Our focus is on space charge interactions mainly and the inclusion of multiple interactions as well as beams with arbitrary transverse aspect ratios is especially important. We then used the analytical tune shifts to derive semi-analytical expressions for the density distribution of tunes assuming that the density is a Gaussian function of the phase-space coordinates. The tune distribution requires an inversion of the functional arguments followed by a numerical interpolation. We emphasize that the tune distribution thus obtained requires no numerical simulations. This is important because the density at the maximum tune shift requires very high sampling of this region and quite often the simulations get the wrong shape of the density in this region. The density is expressed in terms of variables (ξ_x, ξ_y) which are the tune shifts scaled by the maximum tune shifts. Therefore the density $\rho(\xi_x, \xi_y)$ has the same form and shape for both space charge and beam-beam interactions. With the method presented here, we verified that the low order moments of the distribution are preserved in the transformation; exactly in 1D and with a $\sim 2\%$ error in 2D for the zeroth moment, see Table 1 for the other moments. These error could be further reduced by improving the numerical schemes for the function inversion and interpolation. This calculation of the density distribution in tunes will enable a more accurate modeling of Landau damping with space charge and an external nonlinearity such as octupoles as well as the damping with beam-beam interactions.

We checked the tune spread calculations for the IOTA proton ring with simulations using the pyorbit code. At the highest intensities planned with bunched beams, there is substantial emittance blow up and steps will need to be taken to mitigate emittance growth and beam loss. We used a numerical scheme of slow initialization to reduce the growth and prevent beam loss over the short time scale of the simulation. Using this scheme, we found generally good agreement between the footprints calculated by theory and simulation. The expressions for the theoretical footprints developed in this paper should therefore be useful for bench-marking other space charge simulation codes.

Acknowledgments

I thank former undergraduate interns David Feigelson (U Chicago) and Runze Li (UW, Madison; now at Yale) and colleague Francois Ostiguy for their enthusiastic collaboration on a project to model space charge effects in IOTA. I am especially thankful to Runze for writing a library of pyorbit codes needed for modeling IOTA; these codes are available at his github site [22].

Fermilab is operated by Fermi Research Alliance LLC under DOE contract No. DE-AC02CH11359.

References

- [1] D. Mohl, *Landau damping of dipole modes by space charge and octupoles*, CERN/PS-95-08 (DI)
- [2] X. Buffat et al, *Stability diagrams of colliding beams in the Large Hadron Collider*, Phys. Rev. ST Accel. Beams 17, 111002
- [3] V. Shiltsev et al, *Landau Damping of Beam Instabilities by Electron Lenses*, Phys. Rev. Lett. 115, 264801 (2015).
- [4] E. Keil, *Beam-beam dynamics*. No. CERN-SL-94-78-AP. CERN, 1994.
- [5] T. Sen, *Head-on beam-beam interactions on the Tevatron* (unpublished notes), ca. 2003
- [6] T. Sen et al, *Beam - beam effects at the Fermilab Tevatron: Theory*, Phys.Rev.ST Accel.Beams 7 (2004) 041001
- [7] K.Y. Ng, *Distribution of incoherent space charge tune shift for a bi-Gaussian beam*, FERMILAB Report TM-2241 (2004)
- [8] K. Takayama, *A new method for the potential of a 3 dimensional nonuniform charge distribution*, Lett. al Nuovo Cimento, **34**, 196 (1980)
- [9] S. Krishnagopal and R. Siemann, *Bunch Length Effects in the Beam-beam Interaction*, Phys.Rev.D 41 (1990) 2312
- [10] T. Sen. *The beam-beam interaction of finite length bunches in hadron colliders*, FNAL-Pub-00/093-T (2000)
- [11] M. Furman, *The Hourglass reduction factor for asymmetric colliders*, SLAC-ABC-21A (1991)
- [12] T. Sen, *Luminosity and beam-beam tune shifts with crossing angle and hourglass effects in an $e^+ e^-$ colliders*, e-Print: 2208.08615 [physics.acc-ph]
- [13] I. S. Gradshteyn and I. M. Ryzhik, *Table of Integrals, Series and Products* (Academic Press, New York)

- [14] E. Metral and F. Ruggiero, *Stability diagrams for Landau damping with two-dimensional betatron tune spread from both octupoles and nonlinear space charge applied to the LHC at injection*, Proc. EPAC 2004
- [15] V. Danilov and S. Nagaitsev, *Nonlinear Accelerator Lattices with One and Two Analytic Invariants*, Phys. Rev. ST-AB, **13**, 084002 (2010)
- [16] S. Antipov et al, *IOTA (Integrable Optics Test Accelerator): Facility and Experimental Beam Physics Program*, JINST **12**, T03002 (2017)
- [17] J. Jarvis et al, *Experimental demonstration of optical stochastic cooling*, Nature **608**, 287 (2022)
- [18] <https://github.com/PyORBIT-Collaboration/py-orbit>
- [19] R. Li, T. Sen and J.-F. Ostiguy, *Modeling Transverse Space Charge effects in IOTA with pyORBIT*, Fermilab report FERMILAB-TM-2753-AD.
- [20] D. Feigelson, T. Sen, J.-F. Ostiguy and R. Li, *Space Charge Driven Emittance Growth and the Effect of Octupoles in IOTA*, arxiv e-Print: 2112.15306
- [21] F. Schmidt et al, *Code bench-marking for long-term tracking and adaptive algorithms*, Proceedings of HB2016,, p 357 (2016)
- [22] https://github.com/Patchouligoo/pyorbit_iota